Journal of Electronics and Electrical Engineering
https://ojs.wiserpub.com/index.php/JEEE

Research Article

Modeling and Control of the X-Filter for Enhanced Pulp Mill Performance

José M. Campos-Salazar[1*], Felipe Santander[2], Sebastián Larraín[3]

[1] Department of Electronic Engineering, Universitat Politècnica de Catalunya, Barcelona, Spain
[2] Process Control Department, Celulosa Arauco y Constitución S.A., Concepción, Chile
[3] Process Research Department, Bioforest S.A., Concepción, Chile
E-mail: jose.manuel.campos@upc.edu

Received: 21 December 2024; **Revised:** 5 February 2025; **Accepted:** 10 February 2025

Abstract: The dynamic performance of control strategies for an X-filter process is critically analyzed, emphasizing the advantages of model predictive control (MPC) over traditional proportional-integral (PI) control. A detailed simulation model, grounded in the linearized expressions of the X-filter process, was developed using MATLAB-Simulink, with parameters systematically defined and tested under various disturbance scenarios. Key performance indicators, including steady-state behavior, oscillation magnitude, and control effort, were assessed. Results demonstrate that MPC significantly enhances system responsiveness, achieving a steady state more rapidly than PI controllers, with notable reductions in oscillatory behavior across key process variables. Specifically, oscillations in the manipulated variable m_i were effectively mitigated under MPC control, thereby safeguarding hydraulic pump integrity. Statistical analysis of standard deviations for controlled variables revealed that MPC reduces variability in h_1, h_2, and dp by 9%, 24%, and 32% respectively, underscoring its superior ability to maintain stability amidst high-frequency noise and external disturbances. The average position deviation for manipulated variables further illustrates the efficiency of MPC, with reductions of up to 92% in specific instances. Robustness testing confirms MPC's resilience to disturbances in critical input variables, showcasing its adaptability in complex industrial environments. Overall, the findings affirm that MPC not only optimizes set-point tracking but also enhances process control precision, providing a compelling case for its implementation in advanced industrial applications.

***Keywords*:** control systems, disturbance rejection, dynamic analysis, high-frequency noise, model predictive control (MPC), oscillation, PI controller, process variables, simulation results

1. Introduction

The pulp and paper industry is a vital sector that significantly contributes to the global economy, providing essential materials for various applications, including packaging, printing, and writing. Within this industry, the efficiency of production processes directly impacts operational costs and environmental sustainability. Filtration plays a crucial role in the pulp processing stages, particularly in the removal of contaminants and impurities from the pulp slurry, which affects the quality of the final product [1, 2].

In a Kraft pulp mill, the green liquor can be located between the recovery boiler and the causticizing plant and is part of the transition to recover the sodium hydroxide and sodium sulfide used in the cooking process. The production of highly clarified green liquor is particularly beneficial for the unit operations within the white liquor production plant.

DOI: https://doi.org/10.37256/jeee.4120256286

Additionally, the removal of toxic substances from green liquor has become increasingly important for modern evaporation and bleaching processes in pulp mills. One notable example is the accumulation of magnesium in the system resulting from the use of magnesium in the oxygen delignification process. As the magnesium content increases, the settling rate of the green liquor tends to decrease [1].

The X-Filter, a novel cross flow film-forming filter, represents a significant advancement in filtration technology for pulp mills. This filter operates on the principle of crossflow filtration, which facilitates continuous separation of solids from liquids while minimizing the accumulation of retained materials on the membrane surface. As a result, the X-Filter enhances the filtration efficiency and extends the operational lifespan of the filtering media. However, the dynamic nature of pulp processing environments introduces various disturbances and challenges that necessitate robust control strategies to optimize filter performance [2, 3, 4].

Control systems play a pivotal role in managing process variables and ensuring the stability of the filtration operation. Traditional control methods, such as proportional-integral (PI) control, are widely employed in industrial settings; however, they often struggle to cope with the inherent variability and non-linearities present in complex processes like those in pulp mills [5]. This limitation is particularly evident when external disturbances, such as changes in feed consistency or flow rates, disrupt the steady-state operation, resulting in suboptimal performance and increased wear on system components [6].

Model predictive control (MPC) has emerged as a more sophisticated alternative, offering enhanced capabilities for managing complex dynamic systems [7, 8]. By utilizing a model of the process, MPC anticipates future behavior and optimizes control inputs over a finite horizon, effectively addressing the challenges posed by system non-linearities and external disturbances. The application of MPC in the context of the X-Filter presents an opportunity to significantly improve process performance, enabling faster response times, reduced oscillations, and enhanced disturbance rejection capabilities.

This study aims to model the X-Filter process and design a control strategy that leverages MPC to optimize its performance in a pulp mill environment. Through extensive simulations conducted in MATLAB-Simulink, the research will compare the efficacy of the MPC against traditional PI control methods, specifically focusing on critical process variables such as liquid levels ($h_1(t)$ and $h_2(t)$) and pressure differentials ($dp(t)$).

This research not only seeks to establish the X-Filter as a pivotal technology in pulp processing but also aims to demonstrate the superior control capabilities of MPC in managing complex filtration dynamics. The outcomes are expected to have broader implications for the pulp and paper industry, particularly in enhancing process efficiency, reducing operational costs, and improving the sustainability of pulp production.

This article is organized as follows: Section 2 contains the description of the process and the methodology for the modeling, while Section 3 examines and designs the control system in detail. Finally, in Sections 4 and 5, the simulation results are presented, and the study's conclusions are outlined.

2. Material and methods

This section provides a comprehensive description of the process, including a detailed model of the process dynamics.

2.1 *Process description*

The flow of raw green liquor (RGL) and filtered green liquor (FGL) are key components of the process, as illustrated in Figure 1. The process consists of two main operational units: The X-Filter (labeled as A, B, and C) and a storage tank (labeled as D).

The X-Filter comprises three main components:

- A: A pressurized cylindrical tank.
- B: Two filter cloths.

- C: An internal vessel.

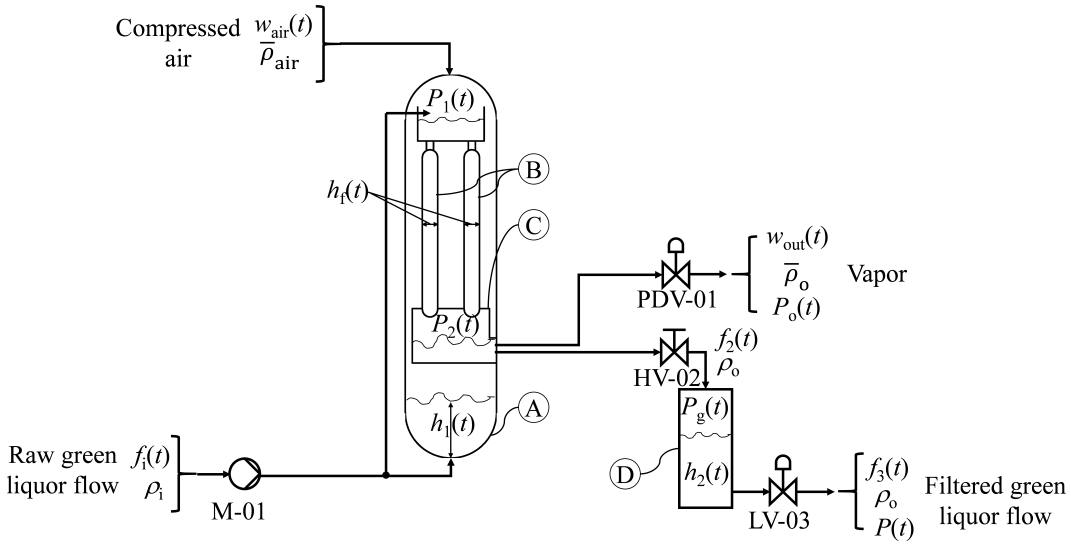

Figure 1. Process diagram of X-Filter process plant

The storage tank (D) is also a pressurized cylindrical tank and is equipped with one inlet pipe and one outlet pipe, while the X-Filter has three inlet pipes and two outlet pipes.

The process involves filtering a stream of RGL, labeled as $f_i(t)$, with a density of ρ_i. As described in [3], $f_i(t)$ is driven by a hydraulic pump and enters the X-Filter from both the top and bottom (refer to Figure 1). The lower inlet generates an upward flow, flooding the X-Filter and allowing the liquor to rise to the upper part. This flow from the lower part is combined with the inlet connected to the upper part, accumulating in an upper vessel within the filter (Figure 1).

Subsequently, $f_i(t)$ passes through two conduction channels located in the lower part of this vessel, eventually reaching the filter cloth in part B. The filter cloth facilitates the filtration of RGL, which then accumulates in the internal vessel (C). Compressed air is introduced through the upper pipe, generating a molar density flow denoted as $w_{air}(t)$ and characterized by $\overline{\rho}_{air}$. This compressed air flow pressurizes the system, with the X-Filter operating at pressure $P_1(t)$ and vessel C at pressure $P_2(t)$ due to the presence of FGL.

Figure 1 also illustrates two outlets from vessel C:

- The first outlet allows a mixture of compressed air and green liquor vapor to escape due to the filtration process. This vapor, with a flow rate denoted as $w_{out}(t)$ and a molar density of $\overline{\rho}_o$, exits the X-Filter at pressure $P_o(t)$.
- The second outlet facilitates the evacuation of FGL, flowing at a rate denoted as $f_2(t)$ with a density of ρ_o, directing it towards D.

To ensure the proper operation of the X-Filter and D in a steady state, it is essential to maintain appropriate levels. The levels of the X-Filter and the D are denoted as $h_1(t)$ and $h_2(t)$, respectively. Additionally, for each filter element, an effective filter level $h_f(t)$ can be defined as the quotient of the filter volume V_f divided by the filter area A_f [9].

The flows $w_{out}(t)$ and $f_2(t)$ are regulated by throttle control valves: control valve PDV-01 manages $w_{out}(t)$, while manual valve HV-02 controls $f_2(t)$. Lastly, the storage tank D operates as a buffer, storing FGL at a flow rate labeled $f_3(t)$ with density ρ_o and pressure $P(t)$. This flow is regulated by control valve LV-03.

2.1.1 *Measurement units*

- Absolute densities (ρ_i, ρ_o): kg/m^3.

- Molar densities ($\overline{\rho}_{air}$, $\overline{\rho}_{o}$): moles/m^3.
- Volumetric flows ($f_i(t), f_2(t), f_3(t)$): m^3/s.
- Mass flows ($w_{air}(t)$, $w_{out}(t)$): kg/s.
- Pressures ($P_1(t)$, $P_2(t)$, $P_o(t)$, $P(t)$): kPa.
- Levels ($h_1(t)$, $h_2(t)$, $h_f(t)$): m.
- Volumes and areas: m^3 and m^2, respectively.

2.1.2 *Filtration process characteristics*

The loss-flow filtration system features a unique design that prevents dirt particles from adhering to the filter cloth (B) during the filtration process. In this system, the green feed liquid flows downwards over the filter element's surface. The pressure difference ($P_1(t)$−$P_2(t)$) generated within the filter element allows a portion of the green liquid to pass through the element, while the remainder continues to flow downwards. This downward flow continuously washes away scum particles from the surface, effectively preventing adhesion [3, 9].

During filtration, small scum particles may enter the pores of the filter element. However, regular washing of the element can prevent this. By maintaining the pressure difference ($P_1(t)$−$P_2(t)$) at zero during brushing, dislodged scum particles are effectively removed by the downward flow of green liquor [3, 9].

For analysis, the process is considered ideal if the entire RGL fully floods the X-Filter without any losses through its walls. Additionally, the filter cloths are assumed to be homogeneous, and it is assumed that all RGL passes through them. Furthermore, D is considered lossless, with its content well-mixed.

2.2 *Process modeling*

This section presents a comprehensive derivation and analysis of the nonlinear and linear dynamic models of the X-Filter plant.

2.2.1 *Nonlinear dynamic model of the X-filter plant*

The RGL filtration process utilizing the X-Filter comprises eight distinct operational stages [1, 3, 9]. This study specifically focuses on two of these stages: RGL impulsion and filtration. Green liquor dregs, a byproduct generated within pulp and paper mills, are typically disposed of in landfills. However, these dregs contain significant concentrations of calcium carbonate, making them a viable candidate for utilization as a raw material in the production of ceramic materials, providing a sustainable alternative to conventional disposal methods [3].

Given that the primary objective of this study is to dynamically model the filtration process, only the RGL pumping, and filtration stages are considered. Based on the schematic of the process (see Figure 1), two main control volumes are identified: X-Filter and D.

A mass balance around the X-Filter yields the following dynamic equation for the level variation within the X-Filter, denoted by $h_1(t)$:

$$\frac{dh_1(t)}{dt} = \frac{1}{\rho_o \cdot A_{Xf}} \cdot (\rho_i \cdot f_i(t) - \rho_o \cdot f_2(t)) \tag{1}$$

where A_{Xf} represents the area of the X-Filter.

The rate of change in vapor flow is described by [10]:

$$\frac{dM(t)}{dt} = \overline{\rho}_{air} \cdot w_{air}(t) - \overline{\rho}_{o} \cdot w_{out}(t) \tag{2}$$

Here, $M(t)$ represents the molar flow rate of vapor (moles/s). Given the low-pressure conditions in the X-Filter, the ideal gas law is applicable to relate moles to pressure $P_2(t)$ [5, 10]:

$$M(t) = \frac{P_2(t) \cdot V}{R \cdot T} \tag{3}$$

In (3), V, R, and T represent constants where V is the vessel volume (m^3), R is the ideal gas constant (J/mol· K), and T is the internal temperature (°C) of the vessel C [5, 10]. By substituting (3) into (2), the mass balance of the X-Filter is obtained as a function of $P_2(t)$:

$$\frac{dP_2(t)}{dt} = \left(\frac{R \cdot T}{V}\right) \cdot (\overline{\rho}_{\text{air}} \cdot w_{\text{air}}(t) - \overline{\rho}_{\text{o}} \cdot w_{\text{out}}(t)) \tag{4}$$

Additionally, the dynamics of the solid particle cake formed on the filter medium can be modeled as follows [1, 9]:

$$\frac{dh_{\text{f}}(t)}{dt} = 2 \cdot \frac{P_1(t) - P_2(t)}{\mu \cdot (R_{\text{f}} - \alpha \cdot c \cdot h_{\text{f}}(t))} \tag{5}$$

The factor of 2 in (5) arises due to the presence of two filtration elements. Here, μ represents the fluid viscosity (N· s/m^2), c the solid concentration in the RGL, R_{f} and α are empirical constants related to the filtration medium.

A mass balance around D is formulated as:

$$\frac{dh_2(t)}{dt} = \frac{1}{A_{\text{D}}} \cdot (f_2(t) - f_3(t)) \tag{6}$$

where A_{D} denotes the cross-sectional area of D (m^2). The flow rates through the control valves and the pump, designated as PDV-01, HV-02, and LV-03 as well as M-01 (see Figure 1), are defined by the following equations for $w_{\text{out}}(t), f_2(t)$, $f_3(t)$ [10, 11]:

$$f_{\text{i}}(t) = k_1 \cdot m_{\text{i}}(t) \cdot \sqrt{h_1(t)} \tag{7}$$

$$w_{\text{out}}(t) = C_{\text{v}_1} \cdot vp_1(t) \cdot \sqrt{P_2(t) \cdot (P_2(t) - P_{\text{o}}(t))} \tag{8}$$

$$f_2(t) = C_{\text{v}_2} \cdot \sqrt{\frac{P_2(t) - P_{\text{g}}(t)}{G_{\text{f}}}} \tag{9}$$

$$f_3(t) = C_{\text{v}_3} \cdot vp_2(t) \cdot \sqrt{\frac{P_{\text{g}}(t) + \rho_{\text{o}} \cdot g \cdot h_2(t) - P(t)}{G_{\text{f}}}} \tag{10}$$

In these equations, k_1 is the gain factor, C_{vx} denotes the valve gain (l/m) where $x \in \{1, 2\}$, $v_{\text{px}}(t)$ is the valve position in per unit (pu), g the gravitational constant (m/s^2), and G_{f} the specific gravity of the FGL.

2.2.2 *Steady-state of the X-filter plant*

As part of the theoretical study for this process, understanding the system's dynamics at steady state and clarifying the linearization process are essential. This regime is determined by setting the derivatives in (1) and (4)–(6) to zero. The resulting steady-state equations are given by (11).

These steady-state conditions enable the calculation of the system's operational points (OPs), given by (12) by solving the equation system in (11). In this context, the variables that are yet to be calculated are the pressures $P_1{}^{ss}$, $P_2{}^{ss}$, $P_g{}^{ss}$, and P^{ss}.

As indicated in (12), the capital letters with a superscript "SS" are used to denote that they correspond to the variables in steady state. In particular, at the point at which the system reaches steady state, these variables become manifest in its dynamics.

$$\begin{cases} \rho_i \cdot k_1 \cdot M_i^{ss} \cdot \sqrt{H_1^{ss}} - \frac{\rho_o \cdot C_{v_2}}{\sqrt{G_f}} \cdot \sqrt{P_2^{ss} - P_g^{ss}} = 0 \\ \overline{\rho}_{air} \cdot W_{air}^{ss} - \overline{\rho}_o \cdot C_{v_1} \cdot VP_1^{ss} \cdot \sqrt{P_2^{ss} \cdot \left(P_2^{ss} - P_o^{ss}\right)} = 0 \\ \frac{P_1^{ss} - P_2^{ss}}{\mu \cdot \left(R_f - \alpha \cdot c \cdot H_f^{ss}\right)} = 0 \\ \frac{C_{v_2}}{\sqrt{G_f}} \cdot \sqrt{P_2^{ss} - P_g^{ss}} - \frac{C_{v_3}}{\sqrt{G_f}} \cdot VP_2^{ss} \cdot \sqrt{P_g^{ss} + \rho_o \cdot g \cdot H_2^{ss} - P^{ss}} = 0 \end{cases} \tag{11}$$

$$\begin{cases} P_1^{ss} = \frac{P_o^{ss}}{2} + \left((0.5 \cdot P_o^{ss})^2 + \left(\frac{W_{air}^{ss} \cdot \overline{\rho}_{air}}{C_{v_1} \cdot VP_1^{ss} \cdot \overline{\rho}_o} \right)^2 \right)^{\frac{1}{2}} \\ P_2^{ss} = P_1^{ss} \\ P_g^{ss} = P_1^{ss} - G_f \cdot H_1^{ss} \cdot \left(\frac{k_1 \cdot M_i^{ss} \cdot \rho_i}{C_{v_2} \cdot \rho_o} \right)^2 \\ P^{ss} = \rho_o \cdot g \cdot H_2^{ss} + \left(\frac{C_{v_2}}{C_{v_3} \cdot VP_1^{ss}} \right)^2 \cdot \left(P_g^{ss} - P_1^{ss} \right) \end{cases} \tag{12}$$

2.2.3 *State-space model of the X-filter plant*

Upon determination of these OPs, the nonlinear model is linearized using a Taylor series expansion around the OPs. The resulting linearized state-space model is expressed as:

$$\begin{cases} \dot{\mathbf{x}}(t) = \mathbf{A_s} \cdot \mathbf{x}(t) + \mathbf{B_s} \cdot \mathbf{u}(t) \\ \mathbf{y}(t) = \mathbf{C_s} \cdot \mathbf{x}(t) + \mathbf{D_s} \cdot \mathbf{u}(t) \end{cases} \tag{13}$$

where the state vector $\mathbf{x}(t) = \left[\widehat{h}_1(t),\ \widehat{h}_2(t),\ \widehat{h}_f(t), \widehat{P}_2(t)\right]^{\mathbf{T}}$, input vector $\mathbf{u}(t) = \left[\widehat{P}_1(t), \widehat{P}_o(t), \widehat{P}_g(t), \widehat{P}(t), \widehat{w}_{air}(t), \widehat{m}_i(t), \widehat{vp}_1(t), \widehat{vp}_2(t)\right]^{\mathbf{T}}$, and output vector $\mathbf{y}(t) = \mathbf{x}(t)$. Symbolically, $\{\mathbf{x}(t), \mathbf{y}(t)\} \in \{\mathbb{R}^4\}$ and $\mathbf{u}(t) \in \{\mathbb{R}^8\}$. The linearized matrices can be found in the Appendix A.

2.2.4 *s-domain model of the X-filter plant*

To facilitate the design of linear compensators that enhance the system's operational efficiency, it is necessary to derive the Laplace domain model of the existing multivariable linear state-space model in (13). The transformation to the complex variable s allows for easier analysis and the design of control systems through transfer functions (TFs), which express the relationship between Laplace-transformed inputs and outputs of the system [12, 13, 14].

By obtaining the model in terms of s, various control techniques can be applied to design compensators or controllers that improve system performance and stability [15]. Using (13), the transformation to the s-domain yields the following:

$$\frac{\mathbf{Y}(s)}{\mathbf{U}(s)} = \mathbf{C_s} \cdot (s \cdot \mathbf{I} - \mathbf{A_s})^{-1} \cdot \mathbf{B_s} + \mathbf{D_s} \tag{14}$$

In this context, $\boldsymbol{I}$ is the identity matrix with the same dimensions as $\mathbf{A_s}$. Equation (14) provides the TFs derived from the state-space model, detailing the relationship between inputs and outputs in the Laplace domain.

The individual TFs, represented as $G_{ij}(s)$, can be extracted from (14). These TFs in (14) represent the interactions between each input and output in the system. Moreover, the complex vectors $\mathbf{Y}(s)$ and $\mathbf{U}(s)$ can be defined as $\mathbf{Y}(s) = [H_1(s), H_2(s), H_f(s), P_2(s)]^T$ and $\mathbf{U}(s) = [P_1(s), P_o(s), P_g(s), P(s), W_{air}(s), M_i(s), VP_1(s), VP_2(s)]^T$, where symbolically $\mathbf{Y}(s) \in \{\mathbb{C}^4\}$ and $\mathbf{U}(s) \in \{\mathbb{C}^8\}$.

3. Control system design

This study synthesizes two types of controllers: three feedback output PI-type linear compensators and a MPC. Notably, the system's output variable corresponding to the $h_f(t)$ level is excluded from this section, as, in practice, this level in X-filters is regulated by rebase and is only relevant within the scope of a broader study.

3.1 *Design of the linear feedback output controllers*

To identify the control plants in the process, it is essential to understand the underlying unit operations. As described in [3, 16], and illustrated in Figure 1, three distinct control loops are identified within the system.

The first control loop governs the regulation of the $h_1(t)$ level, while the second is associated with the filtration process, and the third loop manages the D level, represented by $h_2(t)$. While the control loops for $h_1(t)$ and $h_2(t)$ are relatively straightforward to define, the identification of variables crucial for operating the filtration process is more complex.

To identify these variables, a detailed understanding of the filtration dynamics is required. The loss-flow filtration system is characterized by its ability to prevent dregs from adhering to the filter cloth during operation. During this process, the RGL flows downward across the surface of the filter element. A pressure differential ($\Delta P(t) = P_1(t) - P_2(t)$) is created within the filter element, allowing a portion of the green liquor to pass through the element while the remainder flows downward. This downward flow continuously cleans the element's surface, washing away scum particles and preventing their adhesion [3].

During the filtration process, small dreg particles can infiltrate the element pores. However, this is mitigated through regular flushing, which maintains the pressure differential ($\Delta P(t)$) on both sides of the filter element at zero. The dislodged particles are then removed by the downward flow of green liquor. In this system, filtration capacity is controlled via compressed air, while the flow rate of the green liquor is managed through the liquid level ($h_2(t)$) in the D located at the X-filter outlet [3].

Based on these dynamics and the transfer functions in (14), the process control diagram of the X-filter is derived and depicted in Figure 2. This diagram reveals the three primary control loops in the system:

- Level Controller (LC-01): Regulates $h_1(t)$.
- Level Controller (LC-03): Regulates $h_2(t)$.
- Differential Pressure Controller (DPC-02): Regulates $\Delta P(t)$.

The design of the controllers is explained in subsequent sections. Each compensator to be designed is a PI-type controller, chosen for its simplicity, ease of implementation, and ability to minimize steady-state errors when properly designed [11, 12].

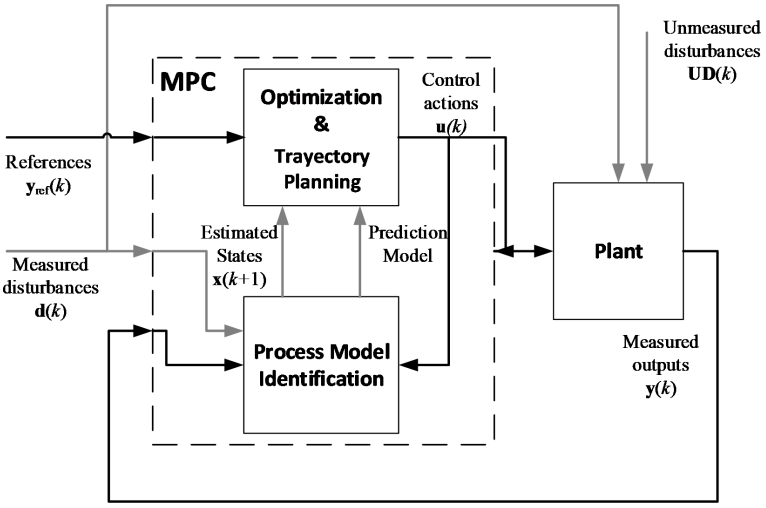

Figure 2. Block diagram representing the MPC

3.1.1 *LC-01 Design*

In the control loop depicted in Figure 3, the measured variable $h_1(t)$ is compared to its reference value $h_1^*(t)$ to generate an error signal. This error signal is then processed by the compensator LC-01. The output of the compensator, denoted as $m_i(t)$, acts as the command signal for the operation of the pump M-01. The compensator LC-01 plays a critical role in achieving the desired control response by regulating the system to meet the specified set point.

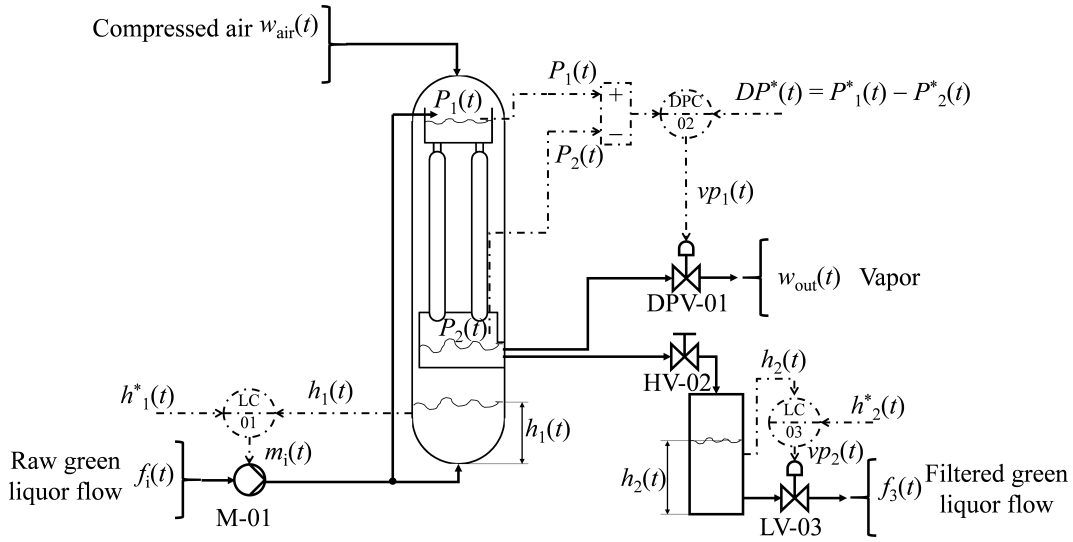

Figure 3. X-Filter process control diagram. Three control loops are identified. Two level controllers, i.e., LC-01 and LC-03 and a differential pressure controller DPC-02

The plant to be controlled in open-loop operation is represented by the TF (from (14)) $G(s)$, which is expressed as:

$$\frac{H_1(s)}{M_i(s)} = G(s) = \frac{K_{12}}{s} \tag{15}$$

where K_{12} can be found in Appendix A.

As shown in (15), the $G(s)$ represents a plant with pure capacitance, characterized by an integrative dynamic. This type of plant behavior is common in process control systems and is well-documented in works such as [10, 11]. Due to the integrative nature of $G(s)$, the direct synthesis method (DSM) is a suitable approach for controller design because of its simplicity and effectiveness. DSM is part of the broader category of model-based control techniques.

For simplicity, the closed control loop associated with the plant $G(s)$ is configured with unitary feedback. The closed-loop TF is then defined as:

$$\frac{H_1(s)}{H_1^*(s)} = Q(s) = \frac{G_c(s) \cdot G(s)}{1 + G_c(s) \cdot G(s)} \tag{16}$$

Here, $G_c(s)$ is the TF of the well-known PI compensator, where k_c and τ_i are the proportional gain and the integral time constant of the compensator, respectively [12].

Using (16), $G_c(s)$ can be derived as part of the DSM, yielding:

$$G_c(s) = \frac{1}{G(s)} \cdot \frac{Q(s)}{1 - Q(s)} \tag{17}$$

To achieve first-order behavior for $G(s)$, the desired closed-loop dynamics are set as:

$$Q(s) = \frac{1}{\tau_r \cdot s + 1} \tag{18}$$

where τ_r is the desired time constant for the process. Substituting $Q(s)$ into (17) gives:

$$G_c(s) = \frac{1}{\tau_r \cdot K_{12}} \tag{19}$$

Based on (19) and following the recommendations of the DSM, the parameters of the compensator $G_c(s)$ are defined as:

$$k_c = 1/(\tau_r \cdot K_{12}); \tau_i = 10 \cdot \tau_r \tag{20}$$

This approach ensures a well-behaved, robust control system tailored to the dynamics of the plant $G(s)$. By utilizing the DSM, the design process remains straightforward, while achieving effective regulation of the process variable $h_1(t)$.

3.1.2 *LC-03 design*

Similar to the previous case (see Figure 3), the control loop in this scenario compares the measured variable $h_2(t)$ with its reference value $h_2{}^*(t)$, generating an error signal. This error signal is then processed by the compensator LC-03, which manipulates the control variable $vp_2(t)$ to directly adjust the throttling of the valve. By modifying the valve opening, the compensator ensures the system maintains the desired set point and achieves the required control response.

The open-loop plant to be controlled, derived from (14) and represented in its canonical form, is defined as:

$$\frac{H_2(s)}{VP_2(s)} = G(s) = -\frac{\frac{K_{25}}{K_{21}}}{\frac{s}{K_{21}} + 1} \tag{21}$$

Here, K_{21} and K_{25} are defined in Appendix A.

As seen in (21), the plant exhibits a first-order dynamic. The corresponding closed-loop control system, with the plant $G(s)$, is configured with unitary feedback. The closed-loop transfer function is expressed as:

$$\frac{H_2(s)}{H_2^*(s)} = Q(s) = \frac{G_c(s) \cdot G(s)}{1 + G_c(s) \cdot G} \tag{22}$$

Here, $G_c(s)$ is the TF of the well-known PI compensator, similar to case before.

Similar to the previous case, the design of the $G_c(s)$ is obtained and defined as:

$$k_c = -1/(\tau_r \cdot K); \tau_i = -\tau \tag{23}$$

where:

$$K = K_{25}/K_{21}; \tau = 1/K_{21} \tag{24}$$

This approach ensures that the designed compensator effectively handles the inverse response of the $G(s)$ plant while maintaining stability and achieving the desired control performance. By properly selecting τ_r, the system response can be tuned to meet specific process requirements.

3.1.3 *DPC-02 design*

This control structure (see Figure 3) employs an indirect regulation of the pressure difference ($\Delta P(t)$) by directly regulating $P_2(t)$, as described by [3]. In this feedback loop, the measured variable $\Delta P(t)$ is compared to its reference value $\Delta P^*(t)$ (where $\Delta P^*(t) = P_1{}^*(t) - P_2{}^*(t)$), generating an error signal. This error signal is processed by the compensator DPC-02, which produces the control signal vp_1 to adjust the valve DPV-01.

The open-loop plant to be controlled, represented in its canonical form, and derived from (14), is defined as follows:

$$\frac{P_2(s)}{VP_1(s)} = G(s) = \frac{\frac{K_{44}}{K_{41}}}{\frac{s}{K_{41}} + 1} \tag{25}$$

where K_{41} and K_{44} can be found in Appendix A.

As shown in (25), TF $G(s)$ represents a first-order dynamic system. Therefore, the closed-loop control diagram for this case is analogous to the ones described for LC-01 and LC-03.

Using DSM applied in the designs of the LC-01 and LC-03 compensators, $G_c(s)$ is derived to regulate $G(s)$. The parameters of the DPC-02 compensator are given by:

$$k_c = -1/(\tau_r \cdot K); \tau_i = -\tau \tag{26}$$

where:

$$K = K_{44}/K_{41}; \tau = 1/K_{41} \tag{27}$$

This approach ensures that the compensator effectively controls $P_2(t)$, enabling proper regulation of the pressure difference ($\Delta P(t)$) while compensating for the inverse response behavior of the system. As with the previous controllers, tuning the parameter τ_r allows for adjustment of the system response to meet desired performance criteria.

3.2 *Overview of model predictive control implementation*

MPC is an advanced control technique that leverages a dynamic process model to predict future behavior and optimize system performance. Unlike traditional controllers, MPC is particularly suitable for handling multivariable systems with constraints, enabling precise and efficient control [8, 17].

The implementation of MPC involves the following steps, illustrated in Figure 2 which shows the MPC configuration:

3.2.1 *Process model identification*

The first step in MPC is to develop an accurate process model, which is critical for reliable predictions of system behavior. This involves:

3.2.1.1 *Data collection*

Process data is collected under varying operating conditions to capture the system's dynamic behavior [18].

3.2.1.2 *Model structure selection*

Discrete state-space models are commonly used for process modeling. These models represent the system in the form of input, output, state, and disturbance vectors as:

$$\begin{cases} \mathbf{x}(k+1) = \mathbf{A}\cdot\mathbf{x}(k) + \mathbf{B}\cdot\mathbf{u}(k) + \mathbf{E}\cdot\mathbf{d}(k) \\ \mathbf{y}(k+1) = \mathbf{C}\cdot\mathbf{x}(k) + \mathbf{D}\cdot\mathbf{u}(k) + \mathbf{F}\cdot\mathbf{d}(k) \end{cases} \tag{28}$$

In this case, $\{\mathbf{A}, \mathbf{B}, \mathbf{C}, \mathbf{D}\} = \{\mathbf{A}_s, \mathbf{B}_s, \mathbf{C}_s, \mathbf{D}_s\}$. Also, from (28):

- $\mathbf{x}(k)$, $\mathbf{u}(k)$, $\mathbf{y}(k)$, $\mathbf{x}(k)$, and $\mathbf{d}(k)$ are the input, output, state, and disturbance vectors, respectively.
- Matrices $\mathbf{A}$, $\mathbf{B}$, $\mathbf{C}$, $\mathbf{D}$, $\mathbf{E}$, and $\mathbf{F}$ define the process dynamics.
- k represents discrete time steps.

3.2.1.3 *Parameter estimation*

- Advanced mathematical methods such as linear regression, least squares, or nonlinear optimization are employed to estimate the parameters of the model.
- These methods aim to align the predicted outputs with actual measured data to minimize prediction errors and achieve high accuracy [18, 19]

3.2.1.4 *Validation*

Validation ensures that the identified model generalizes well to unseen scenarios. A separate dataset is used to compare the model's predictions to actual process outputs, ensuring robustness [18].

3.3 *Optimization process*

Once the process model is identified, MPC employs this model to predict future system behavior and solve an optimization problem at each control interval. The optimization process involves:

3.3.1 *Objective function definition*

The objective is typically to:

- Minimize the deviation of output variables from their reference values.
- Minimize control effort, i.e., the use of manipulated variables.

The general form of the objective function is defined in (29). From here,

- N_p: Prediction horizon.
- N_u: Control horizon.
- $y(k + i)$: Predicted output at time $k + i$.
- $u(k + i)$: Control input at time $k + i$.
- $y_{ref}(k + i)$: Desired output at time $k + i$.

$$J = \sum_{i=0}^{N_p} (y(k+i) - y_{ref}(k+i))^T \cdot \mathbf{Q} \cdot (y(k+i) - y_{ref}(k+i)) + \sum_{i=0}^{N_u-1} u(k+i)^T \cdot \mathbf{R} \cdot u(k+i) \quad (29)$$

- **Q** and **R**: Weighting matrices for outputs and inputs.

3.3.2 *Solving the optimization problem*

The goal is to find the optimal sequence of control actions $u(k)$ that minimizes the objective function J while respecting system constraints (e.g., input/output limits).

3.3.3 *Applying the control action*

- Only the first control action of the optimal sequence is applied to the system. This allows the controller to adapt in real time to changes and disturbances [20].
- The optimization problem is re-solved at every control interval based on new measurements, ensuring continuous adjustments.

3.4 *Control path planning*

Control path planning refers to the generation of a sequence of control actions that guide the system from its current state to a desired state in an optimal and efficient manner. This involves:

3.4.1 *Prediction horizon*

Using the process model, MPC predicts the system's response to various control actions over the prediction horizon.

3.4.2 *Trajectory evaluation*

MPC evaluates multiple potential control trajectories to minimize the tracking error and meet system constraints.

3.4.3 *Trajectory adjustment*

At each control interval, the trajectory is adjusted based on real-time system measurements and conditions [17].

The control path planning process ensures that the system responds dynamically to disturbances while maintaining optimal performance.

3.5 *MPC applied to the X-filter process*

The application of MPC to the X-Filter process is depicted in Figure 4, which is an augmented version of the control diagram in Figure 3. The diagram includes the MPC configuration, which is modeled according to (28) and (29).

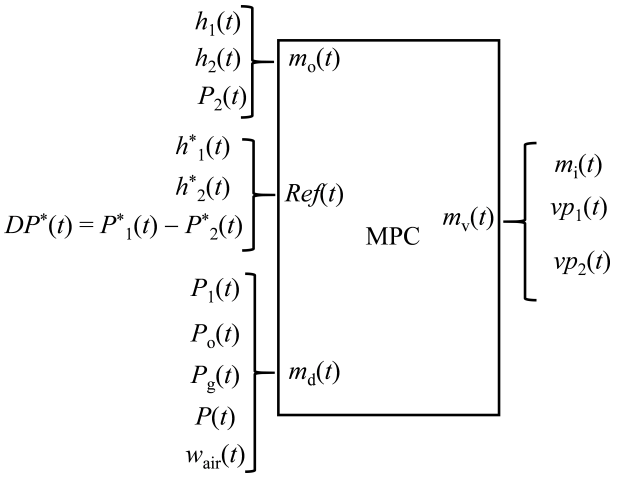

Figure 4. Control diagram of the X-filter process, using an MPC

3.5.1 *Inputs to MPC*

- Measured outputs ($mo(t)$): Real-time measurements of the controlled variables.
- Reference variables ($ref(t)$): Desired output setpoints.
- Measured disturbances ($md(t)$): Disturbances that affect the system.

3.5.2 *Outputs from MPC*

- Manipulated variables ($mv(t)$): Optimal control actions applied to the process.

4. Simulation results

The simulation model adheres to the linearized expression of the X-filter process, as defined in (13), and was implemented using MATLAB-Simulink. The simulation parameters were derived from the constants developed earlier, with their values presented in Table 1. Signals corresponding to disturbance and reference variables are detailed in Table 2. To enhance the analysis and evaluate system robustness comprehensively, high-frequency random noise, modeled as additive white Gaussian noise in per unit (pu), was incorporated. This noise serves to simulate industrial disturbances typically caused by sensor measurement errors, process vibrations, and external perturbations from connected equipment.

Table 1. Variables & parameters in functions of Ks of the process

K-constants	Values
K_{11}	0.005
K_{12}	0.0457
K_{13}	0.021
K_{21}	1.054
K_{22}	1.154
K_{23}	1.355
K_{24}	1.365
K_{25}	1.765
K_{31}	2.045
K_{32}	2.145
K_{33}	2.645
K_{41}	3.021
K_{42}	3.001
K_{43}	3.111
K_{44}	3.121

Table 2. Equivalences between MPC and X-filter variables

MPC variables	X-filter variables
m_o	h_1, h_2, P_2
Ref	h_1^*, h_2^*, DP^*
m_d	$P_1, P_o, P_g, P, w_{air}$

Mathematically, these high-frequency noise disturbances are represented as

$$n(t) = \sum_{i=1}^{m} A_i \cdot \sin\left(2 \cdot \pi \cdot f_i \cdot t + \phi_i\right) \tag{30}$$

where A_i represents the amplitude, f_i the frequency, and ϕ_i the phase of the noise components. These disturbances were intentionally designed to challenge the robustness of the two control strategies, PI and MPC, by introducing varying high-frequency components. This noise allows for a realistic evaluation of each control strategy's ability to suppress the effects of such high-frequency perturbations. The process dynamics described in (13) were modeled alongside the control algorithms, with Figure 4 illustrating the "X-filter" under MPC control and Figure 3 depicting the same process under a PI controller.

During the simulation, the process was assumed to be in a stationary regime, with variables $h_1(t)$, $h_2(t)$, and $\Delta p(t)$ stabilized at steady-state values of 50% for levels and -10 kPa for pressure. The steady-state valve positions for DPV-01 and LV-03 were approximately 86% and 57%, respectively, while the pump speed percentage for M-01 was around 23%. Additionally, key assumptions included P_1 = 150 kPa, P_g = 54 kPa, P_o = 110 kPa, P = 30 kPa, and w_{air} = 650 kg/s.

The impact of high-frequency noise on system performance is evident from an analysis of Figures 5 and 6. While both control strategies are affected by noise, the MPC system exhibits significantly greater noise attenuation. The MPC controller's predictive capability and optimization-based algorithm inherently act as a low-pass filter, effectively minimizing high-frequency oscillations in manipulated variables ($m_i(t)$, $vp_1(t)$, and $vp_2(t)$). This is in contrast to the PI controller, where sinusoidal coupling of high-frequency disturbances with manipulated variables is more pronounced. Such oscillations, when left unmitigated, may adversely impact sensitive equipment such as hydraulic pumps and valves, leading to potential damage and reduced operational efficiency. Quantitatively, the robustness of the MPC system is further validated through reduced oscillation amplitudes and standard deviations in key process variables ($h_1(t)$, $h_2(t)$, and $\Delta p(t)$) compared to the PI controller. The noise mitigation efficiency (η_{noise}) was calculated using the following:

$$\eta_{noise} = 100\% \cdot \frac{\sigma_{PI} - \sigma_{MPC}}{\sigma_{PI}} \tag{31}$$

For $h_1(t)$, the noise mitigation efficiency is 9%, meaning that σ_{MPC} is reduced to 91% of σ_{PI}. For $h_2(t)$, the noise mitigation efficiency is 24%, reducing σ_{MPC} to 76% of σ_{PI}. Finally, for $\Delta p(t)$, the noise mitigation efficiency is 32%, with σ_{MPC} being 68% of σ_{PI}. These values confirm the superior noise suppression capability of MPC over PI, particularly in terms of oscillation amplitude and variability reduction in key process variables.

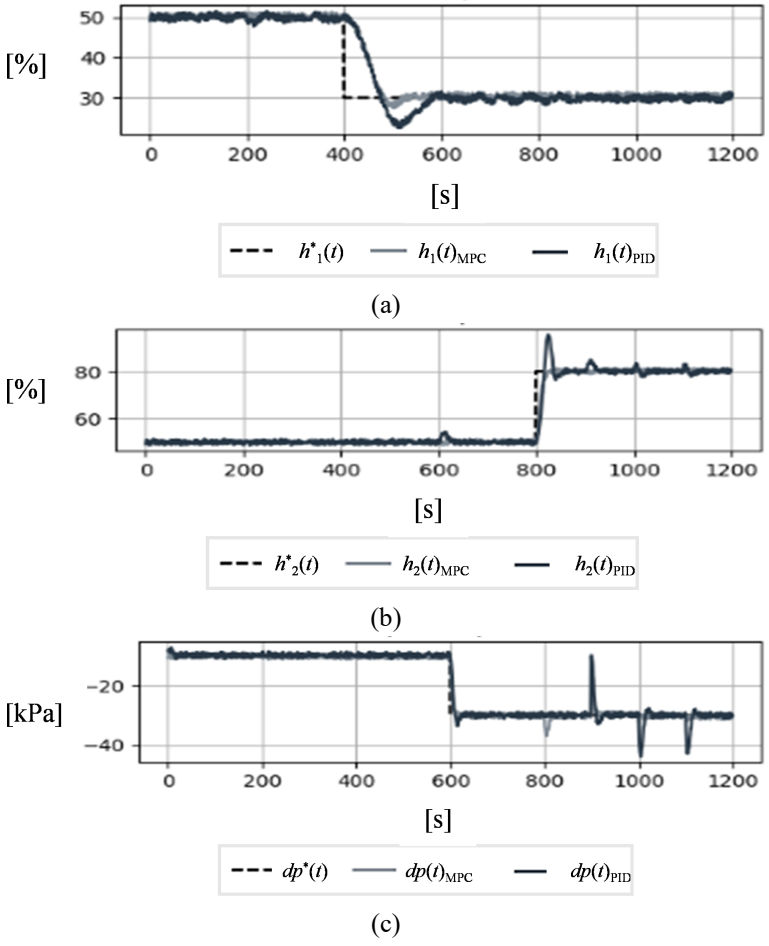

Figure 5. Simulation results under transients. (**a**) $h_1(t)$. (**b**) $h_2(t)$. (**c**) $dp(t)$

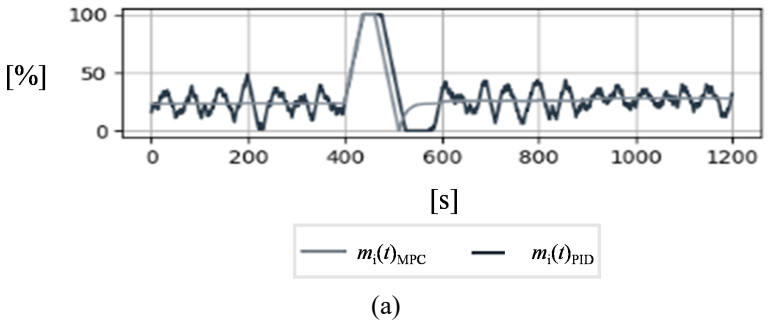

Figure 6. *Cont.*

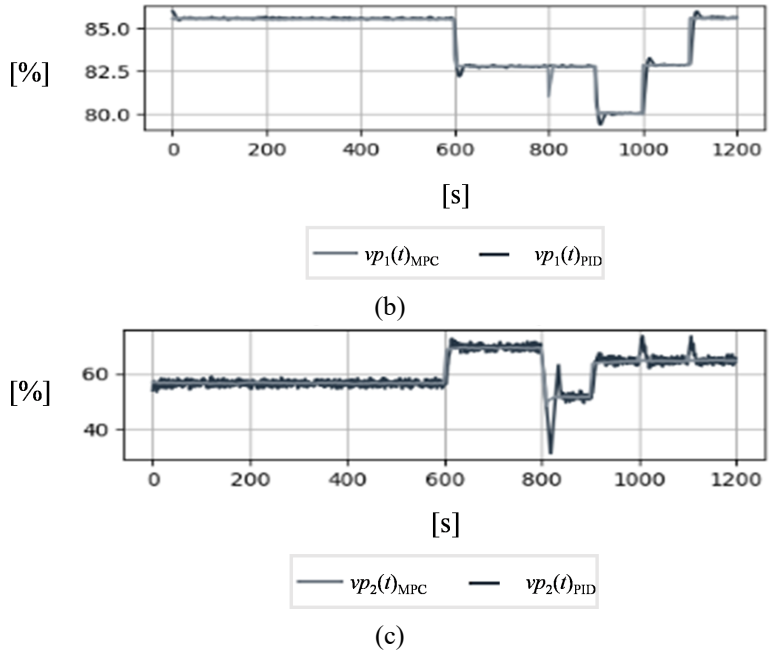

Figure 6. Simulation results of the manipulated variables, under transient. (**a**) $m_i(t)$. (**b**) $vp_1(t)$. (**c**) $vp_2(t)$

The dynamic behavior of the process, as observed in the state variables $h_1(t)$, $h_2(t)$, and $\Delta p(t)$, is detailed as follows. At $t = 40$ s, $h_1(t)$ undergoes a perturbation, dropping from 50% to 30%. The steady state is restored faster under MPC control (56.4 s) than with PI (67.7 s). At $t = 60$ s, $\Delta p(t)$ undergoes a vacuum increase, reaching −30 kPa. The oscillation with MPC is reduced to 4%, compared to 13% under PI control, while steady-state recovery is faster with MPC (62.3 s vs. 66.3 s). At $t = 80$ s, $h_2(t)$ increases from 50% to 80%. The oscillation is significantly lower under MPC (0.65%) compared to PI (19.45%), and steady-state recovery is quicker (83.5 s vs. 93.7 s).

The behavior of manipulated variables further highlights the contrast between the two controllers. With PI control, sinusoidal coupling is observed in $m_i(t)$, $vp_1(t)$, and $vp_2(t)$, likely due to high-frequency noise. These oscillations are absent in the MPC-controlled system, where smoother trajectories for manipulated variables are evident. Figure 6 highlights this difference, with MPC demonstrating its ability to mitigate high-frequency perturbations effectively.

System robustness is further validated through disturbance tests in $P_1(t)$, $P_g(t)$, $P_o(t)$, $P(t)$, and $w_{air}(t)$. MPC maintains superior control stability and performance, as demonstrated by the reduced variability in critical process variables (Figures 7 and 8). The probability density function of the standard deviation for the controlled variables confirms that MPC achieves notable reductions in variability, with improvements of 9%, 24%, and 32% for $h_1(t)$, $h_2(t)$, and $\Delta p(t)$, respectively. These calculations confirm the enhanced robustness of MPC, particularly in handling industrial noise and disturbances.

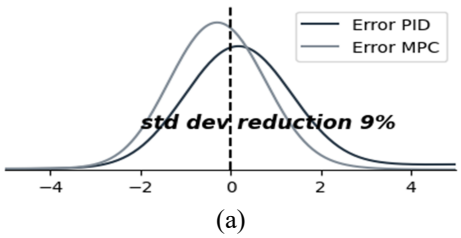

Figure 7. *Cont.*

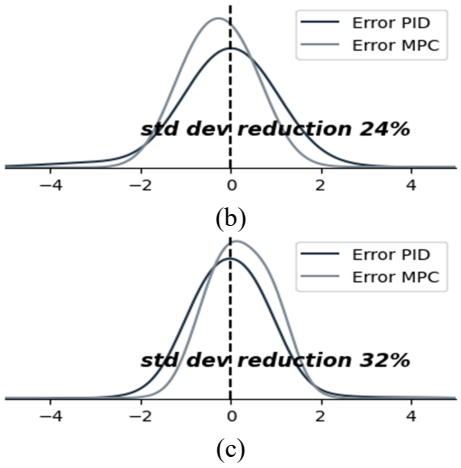

Figure 7. Probability density function of the standard deviation. (**a**) h_1. (**b**) h_2. (**c**) dp

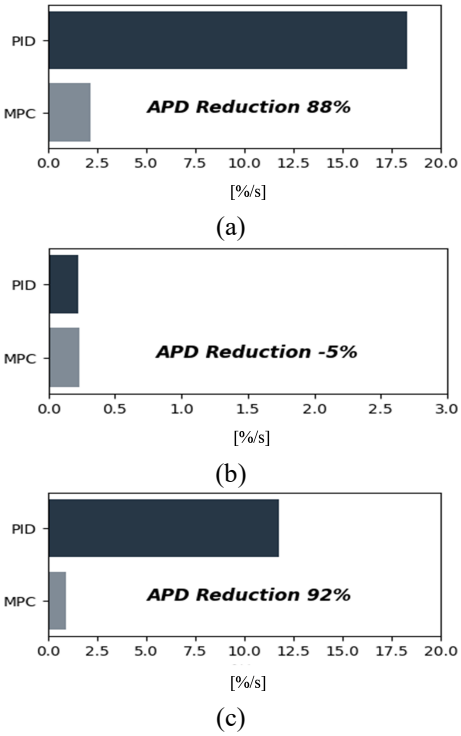

Figure 8. Probability density function of the standard deviation. (**a**) m_i. (**b**) vp_1. (**c**) vp_2

5. Conclusions

The simulation results of the X-filter process, evaluated under both model predictive control (MPC) and proportional-integral (PI) controllers, underscore an appropriate performance, robustness, and industrial relevance of the MPC approach in managing complex, nonlinear systems with inherent dynamics. This study provides a quantitative and qualitative assessment of key process variables—$h_1(t)$, $h_2(t)$, and $\Delta p(t)$—demonstrating the MPC's superiority in achieving precision control, faster response times, and enhanced disturbance rejection compared to traditional PI control strategies.

Dynamic performance comparisons reveal that the MPC controller significantly outperforms the PI controller in terms of both transient and steady-state behavior. For instance, the steady-state response for $h_1(t)$ under MPC was achieved approximately 11.3 s faster than under PI control, showcasing its superior capability to quickly stabilize the process after disturbances. Additionally, MPC demonstrated a dramatic reduction in oscillation amplitudes, with $h_1(t)$ oscillations reduced from 25% under PI control to 8.63% under MPC, and $\Delta p(t)$ oscillations reduced from 13% to 4%. Such improvements in control precision are critical in ensuring process stability, minimizing energy consumption, and avoiding detrimental mechanical stress on industrial components.

The robustness of MPC was further validated through the introduction of high-frequency noise, modeled as additive white Gaussian noise, to simulate real-world industrial disturbances, including sensor inaccuracies, mechanical vibrations, and external perturbations from auxiliary equipment. The MPC effectively mitigated the impact of noise, acting as a dynamic low-pass filter for manipulated variables ($m_i(t)$, $vp_1(t)$, and $vp_2(t)$) and reducing sinusoidal coupling effects, which were pronounced in the PI-controlled system. This noise rejection capability is not only essential for maintaining control stability but also for extending the operational lifespan of critical equipment such as hydraulic pumps and valves by minimizing wear and tear induced by oscillatory inputs.

Sensitivity analysis of the standard deviations (σ) of key controlled variables provides a quantitative measure of the performance enhancements achieved with MPC. For $h_1(t)$, $h_2(t)$, and $\Delta p(t)$, MPC achieved variability reductions of 9%, 24%, and 32%, respectively, compared to PI control. These reductions highlight the system's improved stability, precision in set-point tracking, and resilience against perturbations. Furthermore, the analysis of average position deviation (APD) revealed that MPC effectively coordinated control actions among the manipulated variables. For instance, APD reductions for $m_i(t)$ and $vp_2(t)$ were 88% and 92%, respectively, demonstrating smoother and more efficient control action trajectories. While $vp_1(t)$ exhibited a slight increase in APD, this trade-off was acceptable given the substantial overall performance improvements across other variables, further validating the robustness of the MPC design.

The study also incorporated a comprehensive sensitivity analysis to evaluate the MPC's adaptability to perturbations in system parameters and input disturbances, including $P_1(t)$, $P_g(t)$, $P(t)$, and $w_{air}(t)$. The results confirmed that MPC exhibited superior disturbance rejection and maintained stable control performance even under significant parameter variations, a critical requirement for modern industrial processes subject to fluctuating operational conditions. This sensitivity analysis demonstrates MPC's robustness and capability to adapt to varying system dynamics without compromising control performance, positioning it as an ideal solution for complex and dynamic industrial environments.

In conclusion, the findings of this study establish model predictive control as a technologically advanced and robust alternative to traditional PI controllers in regulating the X-filter process. By achieving faster response times, substantial reductions in oscillations, superior disturbance rejection, and improved equipment longevity, MPC positions itself as an indispensable technology for optimizing performance in highly dynamic and complex industrial applications. Furthermore, its adaptability to high-frequency noise and system parameter variations ensures its applicability in a wide range of operational scenarios.

Future research should focus on real-time implementation strategies, integration of adaptive control techniques, and experimental validation in industrial-scale environments to further extend the capabilities of MPC. Additionally, exploring hybrid control methodologies that combine MPC with machine learning-based predictive analytics may offer transformative advancements in optimizing nonlinear process control systems.

Conflict of interest

There is no conflict of interest for this study.

Appendix A

The matrix in (13) can be defined as:

$$\mathbf{A_s}=\begin{bmatrix}0 & 0 & 0 & K_{11}\\ 0 & -K_{21} & 0 & K_{22}\\ 0 & 0 & K_{31} & -K_{32}\\ 0 & 0 & 0 & -K_{41}\end{bmatrix}$$

$$\mathbf{B_s}=\begin{bmatrix}0 & 0 & K_{11} & 0 & 0 & K_{12} & 0 & 0\\ 0 & 0 & -K_{23} & K_{24} & 0 & 0 & 0 & -K_{25}\\ K_{32} & 0 & 0 & 0 & 0 & 0 & 0 & 0\\ 0 & K_{42} & 0 & 0 & K_{43} & 0 & -K_{44} & 0\end{bmatrix} \tag{A1}$$

$$\mathbf{C_s}=\mathbf{I}_{4\times4}, \mathbf{D_s}=\mathbf{0}_{4\times8}$$

and the matrices $\mathbf{I}_{4\times4}$ and $\mathbf{0}_{4\times8}$ represent the identity matrix of size 4×4 and the null matrix of size 4×8, respectively. Symbolically, $\{\mathbf{A_s}, \mathbf{C_s}\} \in \mathscr{M}_{4\times4}\{\kappa\}$ and $\{\mathbf{B_s}, \mathbf{D_s}\} \in \mathscr{M}_{4\times8}\{\kappa\}$.

The Ks constants cab de found and described as follows:

$$\begin{cases}
K_{11}=0.5\cdot\dfrac{C_{v_2}}{A_{Xf}\cdot\sqrt{G_f\cdot\left(P_2^{ss}-P_g^{ss}\right)}}\\
K_{12}=\dfrac{k_1\cdot\rho_i\cdot\sqrt{H_1^{ss}}}{\rho_o\cdot A_{Xf}}\\
K_{21}=0.5\cdot\dfrac{\rho_o\cdot g\cdot C_{v_3}\cdot VP_2^{ss}}{A_D\cdot\sqrt{G_f\cdot\left(P_g^{ss}+\rho_o\cdot g\cdot H_2^{ss}-P^{ss}\right)}}\\
K_{22}=0.5\cdot\dfrac{C_{v_2}}{A_D\cdot\sqrt{G_f\cdot\left(P_2^{ss}-P_g^{ss}\right)}}\\
K_{23}=\dfrac{0.5}{A_D\cdot\sqrt{G_f}}\cdot\left(\dfrac{C_{v_2}}{\sqrt{P_2^{ss}-P_g^{ss}}}+\dfrac{C_{v_3}\cdot VP_2^{ss}}{\sqrt{P_g^{ss}+\rho_o\cdot g\cdot H_2^{ss}-P^{ss}}}\right)\\
K_{24}=0.5\cdot\dfrac{C_{v_3}\cdot VP_2^{ss}}{A_D\cdot\sqrt{G_f\cdot\left(P_g^{ss}+\rho_o\cdot g\cdot H_2^{ss}-P^{ss}\right)}}\\
K_{25}=\dfrac{C_{v_3}}{A_D}\cdot\sqrt{\dfrac{P_g^{ss}+\rho_o\cdot g\cdot H_2^{ss}-P^{ss}}{G_f}}\\
K_{31}=2\cdot\dfrac{\alpha\cdot c\cdot\left(P_1^{ss}-P_2^{ss}\right)}{\mu\cdot\left(R_f-\alpha\cdot c\cdot H_f^{ss}\right)^2}\\
K_{32}=\dfrac{2}{\mu\cdot\left(R_f-\alpha\cdot c\cdot H_f^{ss}\right)}\\
K_{41}=0.5\cdot\left(\dfrac{R\cdot T}{V}\right)\cdot\left(\dfrac{C_{v_1}\cdot VP_1^{ss}\cdot\overline{\rho}_o\cdot\left(2\cdot P_2^{ss}-P_o^{ss}\right)}{\sqrt{P_2^{ss}\cdot\left(P_2^{ss}-P_o^{ss}\right)}}\right)\\
K_{42}=0.5\cdot\left(\dfrac{R\cdot T}{V}\right)\cdot C_{v_1}\cdot VP_1^{ss}\cdot\overline{\rho}_o\cdot\sqrt{\dfrac{P_2^{ss}}{P_2^{ss}-P_o^{ss}}}\\
K_{43}=\left(\dfrac{R\cdot T}{V}\right)\cdot\overline{\rho}_{air}\\
K_{44}=\left(\dfrac{R\cdot T}{V}\right)\cdot C_{v_1}\cdot\overline{\rho}_o\cdot\sqrt{P_2^{ss}\cdot\left(P_2^{ss}-P_o^{ss}\right)}
\end{cases} \tag{A2}$$

References

[1] J. R. Couper, W. R. Penney, and J. R. Fair, *Chemical Process Equipment—Selection and Design*, Revised 2nd Ed. Amsterdam, The Netherlands: Gulf Professional Publishing, 2009.

[2] R. Bandekar, A. Oldmark, M. Lindstrom, L. Kallen, J. Liedberg, J. Foan, et al., "Crossflow filtration of green liquor for increased pulp production, improved green liquor quality, and energy savings," *Tappi J.*, vol. 19, no. 10, pp. 527–538, Oct. 2020.

[3] R. Lavikainen and M. Fukuzawa, "Green liquor clarification using X-filter plant: Falling film type cross-flow filtration process," *Jpn. Tappi J.*, vol. 49, no. 2, pp. 305–310, Feb. 1995.

[4] D. L. Schütz, *Handbook of Wood Processing: Pulp & Paper*. New York, NY, USA: SCOR Global P&C, Jan. 2022.

[5] W. L. Luyben, *Process Modeling, Simulation and Control for Chemical Engineers*, Subsequent ed. New York, NY, USA: McGraw-Hill College, 1989.

[6] K. Ogata, *Modern Control Engineering*. Boston, MA, USA: Pearson, 2009.
[7] E. F. Camacho and C. B. Alba, *Model Predictive Control*. New York, NY, USA: Springer Science & Business Media, 2013.
[8] D. Q. Mayne, J. B. Rawlings, C. V. Rao, and P. O. M. Scokaert, "Constrained model predictive control: Stability and optimality," *Automatica*, vol. 36, no. 6, pp. 789–814, Jun. 2000.
[9] P. Sedin and H. Theliander, "Filtration properties of green liquor sludge," *Nord. Pulp Pap. Res. J.*, vol. 19, no. 1, pp. 67–74, Jan. 2004.
[10] C. A. Smith and A. B. Corripio, *Principles and Practice of Automatic Process Control*, 2nd ed. New York, NY, USA: Wiley, 1997.
[11] W. L. Luyben, *Process Modeling, Simulation and Control for Chemical Engineers*, Subsequent ed. New York, NY, USA: McGraw-Hill College, 1989.
[12] K. Ogata, *Modern Control Engineering*. Boston, MA, USA: Pearson, 2009.
[13] W. L. Brogan, *Modern Control Theory*. Upper Saddle River, NJ, USA: Prentice Hall, 1991.
[14] *The Control Handbook (Three Volume Set)*. Boca Raton, FL, USA: CRC Press, 2018.
[15] A. Menéndez and S. Simón, *Contribution to the Control of the Three-Level DC/AC Converter*. Barcelona, Spain: Universitat Politècnica de Catalunya, 2004.
[16] J. G. Bralla, *Handbook of Manufacturing Processes—How Products, Components and Materials Are Made*, 1st Ed. New York, NY, USA: Industrial Press, Inc., 2007.
[17] J. M. Maciejowski, *Predictive Control with Constraints*, 1st ed. Harlow, England; New York, NY, USA: Pearson, 2000.
[18] L. Ljung, *System Identification: Theory for the User*, 2nd ed. Upper Saddle River, NJ, USA: Pearson, 1998.
[19] O. Nelles, *Nonlinear System Identification: From Classical Approaches to Neural Networks and Fuzzy Models*. New York, NY, USA: Springer Science & Business Media, 2001.
[20] J. B. Rawlings and D. Q. Mayne, *Model Predictive Control: Theory and Design*. Madison, WI, USA: Nob Hill Publishing, 2009.